Geoderma Regional 2–3 (2014) 21–31

Contents lists available at ScienceDirect

Geoderma Regional

journal homepage: www.elsevier.com/locate/geodrs

Mapping soil salinity changes using remote sensing in Central Iraq

Weicheng Wu [a,*], Ahmad S. Mhaimeed [b], Waleed M. Al-Shafie [c], Feras Ziadat [a], Boubaker Dhehibi [a], Vinay Nangia [a], Eddy De Pauw [a]

[a] International Center for Agricultural Research in the Dry Areas (ICARDA)/CGIAR, Amman, Jordan
[b] College of Agriculture, Baghdad University, Iraq
[c] Ministry of Agriculture (MoA), Baghdad, Iraq

ARTICLE INFO

Article history:
Received 4 April 2014
Received in revised form 16 September 2014
Accepted 17 September 2014
Available online 22 September 2014

Keywords:
Salinity dynamics
Multiyear maxima-based modeling
Multitemporal remote sensing
Soil salinity models
Quantification in space and time

ABSTRACT

Salinization is a common problem for agriculture in dryland environments and it has greatly affected land productivity and even caused cropland abandonment in Central and Southern Iraq. Hence it is of pressing importance to quantify the spatial distribution of salinity and its changing trend in space and time and ascertain the driving forces thereof. This study aims at such a diachronic salinity mapping and analysis using multitemporal remote sensing taking a pilot site, the Dujaila area in Central Iraq, as an example. For this purpose, field survey and soil sampling were conducted in the 2011–2012 period, and a multitemporal remote sensing dataset consisting of satellite imagery dated 1988–1993, 1998–2002, and 2009–2012 was prepared. An innovative processing approach, the multiyear maxima-based modeling approach, was proposed to develop remote sensing salinity models. After evaluation of their suitability, the relevant models were applied to the images for multitemporal salinity mapping, quantification, and change tracking in space and time. The driving causes of salinization in the study area were evaluated. The results reveal that the developed salinity models can reliably predict salinity with an accuracy of 82.57%, indicating that our mapping methodology is relevant and extendable to other similar environments. In addition, salinity has experienced significant changes in the past 30 years in Dujaila, especially, very strongly salinized land got continuously expanded, and all these changes are related to land use practices and management of farmers, which are closely associated with the macroscopic socioeconomic environment of the country.

1. Introduction

Salinity is a problematic issue for agriculture in the Mesopotamian Plain, Iraq since about 2300–2400 BC (Dieleman, 1963; Schnepf, 2004; FAO, 2011) and has become more severe in the recent decades. It is reported that approximately 60% of the cultivated land has been seriously affected by salinity, and 20–30% has been abandoned in the past 4000 years (Buringh, 1960; FAO, 2011) due to irrational land management (e.g., overirrigation and poor drainage) and other natural factors (e.g., flooding, drought, and impermeability of the underlying formation). It is clear that the arable agricultural land would further dwindle in Mesopotamia because of such land degradation, and might be exacerbated by climate change, and food security would face harsh challenge in the country. It is hence of prime importance to quantify the salt-affected land, assess its change trend in space and time, and understand the causes of salinization in order to provide relevant reference for the local and central governments for their sustainable agriculture development and land management in the future.

In regard of the salinization in Central and Southern Iraq, several authors, for example, Jacobsen and Adams (1958), Buringh (1960), Dieleman (1963), Al-Layla (1978), Al-Mahawili (1983) and Abood et al. (2011) have conducted studies and assessments. These assessments allow us to have a general understanding of salinity in the Mesopotamian Plain. International organizations such as FAO and UNESCO (United Nations Educational, Scientific and Cultural Organization) together with the Ministry of Agriculture (MoA) of Iraq have carried out soil classification and mapping in 1960 (Buringh, 1960). FAO (2008) investigated briefly the salinity severity in Western Asia including Iraq. However, the outdating of maps and their extremely low resolution (e.g., 4–10 km in pixel size) cannot meet the requirement of farm-level or household-level land management and for salinity control. Therefore, it is essential to produce salinity maps with higher resolution, higher accuracy and reliability to meet the urgent need of farmers and governments.

Salinity assessment and mapping are traditionally conducted by soil surveys and interpolation of analytical results of soil samples. However, such conventional means of soil survey requires a great deal of time (Ghabour and Daels, 1993) and funding investment. Fortunately, a significant progress has been made in this field thanks to the development of remote sensing technology in the recent decades, which offers a possibility for mapping and assessing salinity processes more efficiently and economically (Garcia et al., 2005). In fact, since the 1970s, a number of authors namely Hunt et al. (1972), Driessen and Schoorl (1973), Golovina et al. (1992), Steven et al. (1992), Mougenot et al. (1993),

* Corresponding author at: 11 Avenue Léon Gourdault, 94600 Choisy-Le-Roi, France.
E-mail address: wuwc123@gmail.com (W. Wu).

http://dx.doi.org/10.1016/j.geodrs.2014.09.002
2352-0094/

Rao et al. (1995), Metternicht (1998), Metternicht and Zinck (2003), Shao et al. (2003), Douaoui et al. (2006), Farifteh et al. (2006, 2007), Fernández-Buces et al. (2006), Brunner et al. (2007), Rodríguez et al. (2007), Eldeiry and Garcia (2010), Furby et al. (2010) and so on have investigated saline soil-related spectral features and radar signatures, and obtained a number of interesting results, for example, the relationships between vegetation indices and soil salinity (Steven et al., 1992; Huete et al., 1997; Garcia et al., 2005; Al-Khaier, 2003; Brunner et al., 2007; Lobell et al., 2010; Iqbal, 2011; Zhang et al., 2011). Some authors have argued for the possibility to assess salinity using the moisture content indicator, NDII (Normalized Difference Infrared Index, Hardisky et al., 1983), and the thermal band (Metternicht and Zinck, 1996, 2003; Goossens and van Ranst, 1998; Iqbal, 2011). Recently, Douaoui et al. (2006), Fernández-Buces et al. (2006), Farifteh et al. (2007), Eldeiry and Garcia (2010) and Hu et al. (2014) have proposed respectively the regression-Kriging method, combined spectral response index (COSRI) and best band combination including vegetation index for salinity classification and spatial variability modeling. Others have even discussed the potential to use SAR (Synthetic Aperture Radar) backscatter coefficients to characterize soil electrical conductivity (Singh and Srivastav, 1990; Singh et al., 1990; Taylor et al., 1996; Metternicht, 1998; Shao et al., 2003).

These studies illustrate not only the advantage, feasibility and great potential of remote sensing and GIS in salinity mapping and assessment but also challenges to which we need to pay attention. Firstly, salt concentrated in subsoil is not easily detected by optical remote sensing (Farifteh et al., 2006); even in the topsoil (surface), if the salt content is below 10–15%, it is difficult to be discriminated from other soil surface components (Mougenot et al., 1993); however, reflectance increases with the increase in quantity of salts at the terrain surface, and this is particularly true for the blue band, in which the interference caused by ferric oxides is masked (Metternicht and Zinck, 2003). In fact, salt-affected soils show relatively higher spectral response in the visible and near-infrared regions of the spectrum than non-saline soils, and strongly saline–sodic soils present higher spectral response than moderately saline–sodic soils (Rao et al., 1995; Metternicht and Zinck, 2003). Secondly, the moisture in soil contributes to the decrease in reflectance in the middle- and near-infrared bands (Epema, 1990; Mougenot et al., 1993), which can easily lead to misinterpretation of salinity if just based on reflectance or vegetation indices. Thirdly, halophyte vegetation and even salt-tolerant crops such as barley, cotton, and alfalfa can modify the overall spectral response pattern of salt-affected soils, especially in the green and red bands (Rao et al., 1995; Metternicht, 1998).

We understood from the above brief review that remote sensing is a promising tool, especially, for large-scale salinity assessment. The outcomes of other authors such as relationships established between vegetation indices, moisture index (e.g. NDII), land surface temperature (LST, from the thermal band) and soil salinity will be useful if they can be ascertained. However, care should be taken to work out a reasonable approach for salinity quantification by taking the above challenges into account. In this context, the main objectives of this study are to propose an integrated approach for soil salinity mapping and assessment, track the change trend of the salt-affected soils in space and time, and ascertain the role of anthropogenic land use practice and management in the salinization processes. The Dujaila site, a severely salt-affected area in Central Iraq (Fig. 1), was selected as a pilot site to demonstrate the development procedure of the integrated mapping approach and its application for salinity change trend tracking.

2. Materials and methods

2.1. Study site

The Dujaila area, located between the Tigris River (north) and the Gharraf River (southwest), and administratively in the Wasit Governorate (Fig. 1) in Central Iraq, is the site where the largest Land Settlement Project started in 1946 as a model and experiment in Iraq after the Second World War (Dieleman, 1963). The total project area is around 99,000 ha including irrigated and non-irrigated land which can be further divided into three zones: reclaimed, semi-reclaimed and non-reclaimed. In the beginning of the project, with the formation of the new irrigation network for reclamation, salinity became worse due to lack of drainage system (Dieleman, 1963). That is why a number of experiments on salinity control by drainage, leaching and cultivation of salt-tolerant crops were conducted in the 1954–1959 period (Dieleman, 1963) and the successful experience was implemented and extended to the whole area. Land reclamation was not stopped until 1983.

The soil in the study site is mainly alluvial silty loam (locally silty clay loam) containing about 26–27% of lime and 0.4–2.5% of gypsum (Dieleman, 1963). According to its origin, the soil is Fluvisols; however, most of the soil is salinized, and locally, strongly salinized, and hence can be also classified as Solonchak or Solonetz in terms of the World Reference Base for Soil Resources (WRB). The measurements of Dieleman (1963) revealed that the surface soil (0–30 cm in depth) had a salinity of about 65 deci-Siemens per meter (denoted as dS/m in the following sections).

The Dujaila area belongs to a subtropical climate zone, characterized by short cool winter and long hot summer. Rainfall is concentrated in winter and spring from November to March with an average annual rainfall of about 141 mm in the past 60 years (measured at the adjacent station, Al-Hay). Winter is cool and short with a mean temperature of 12 °C from December to February. Summer is dry and hot to extremely hot with the maximum mean temperature of 45 °C in July and August.

The crops cultivated are wheat, barley and vegetables in winter and cotton, maize, millet, sorghum and sunflower in summer.

2.2. Field investigation and data

To map salinity, field survey is fundamental and essential. The survey campaign including soil sampling, measurement of EM38-MK2 (briefed as EM38, an electromagnetic instrument made by Geonics Ltd to measure soil electrical conductivity), land use/cover investigation and soil chemical analysis in laboratory was conducted during the October 2011 to June 2012 period. Soil samples included 15 surface (0–30 cm in depth) and 5 profile (0–150 cm) samples. Soil profiles were dug on October 19–21, 2011 and sampled at horizons of 0–30 cm, 50–70 cm, 90–110 cm, and 120–150 cm. Surface soil samples were obtained using auger in the places where EM38 measurements were also conducted on March 25–28, 2012 (4–6 days after rainfall events) and on June 28–July 04, 2012 (dry season after harvesting but before summer irrigation). The five profiles were revisited with EM38 measurements on March 25–28, 2012 due to the late arrival of the latter.

As designed, both vertical and horizontal EM38 readings (denoted respectively as EM_V and EM_H) were taken in plots (1×1 m^2) distributed at three corners of a triangle with a distance of about 15–20 m from each other. The averaged value of the three corner plots was regarded as the representative of the observation point in the center of the triangle. The objective of this treatment is to have more comparability between the field sampled data and the satellite images (with pixel size of 6.5–30 m). The electrical conductivity (EC) of 20 soil samples analyzed using 1:1 dilute method in laboratory and 62 pairs of EM_V and EM_H reading data were made available for this study.

The sampling locations (e.g., each triangle) were randomly selected depending on the accessibility but the variation of the field conditions such as salinity level, crop health and land use types was fully covered. The distribution of the sampling plots is shown in Fig. 2.

A multitemporal dataset mainly composed of Landsat TM (Thematic Mapper) and ETM+ (Enhanced Thematic Mapper Plus) images in the frame of 167-38 (Table 1), one scene of SPOT image dated March 28, 2010 and one RapidEye image dated April 22, 2012 were also acquired.

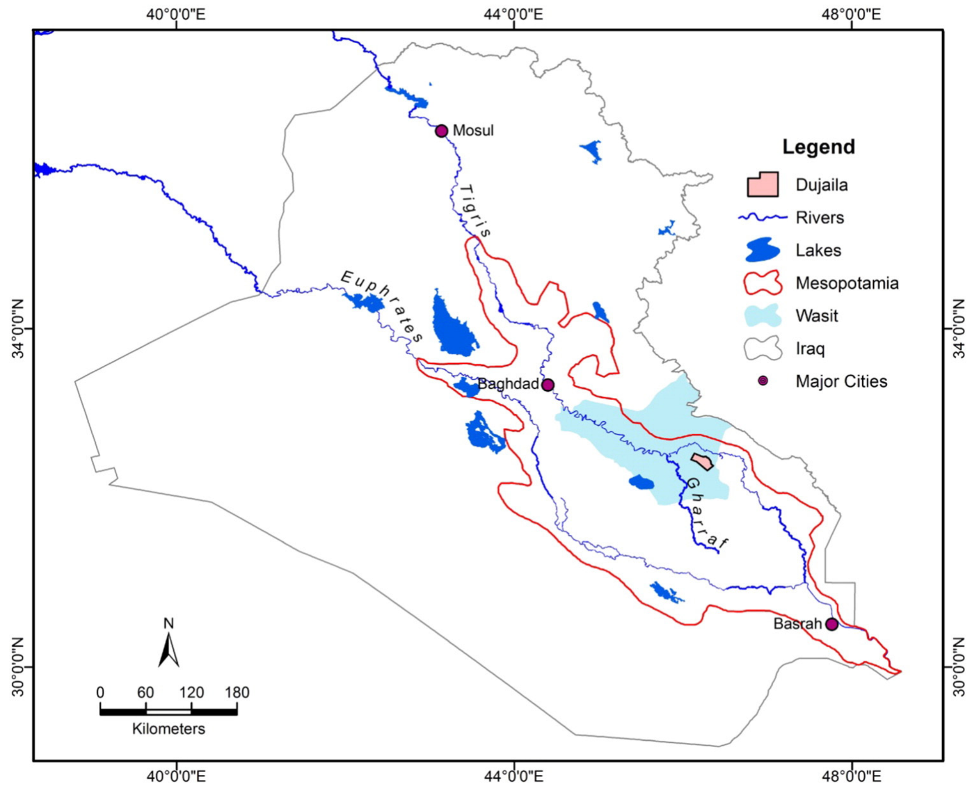

Fig. 1. Location of the study area, Dujaila, in Mesopotamia, Iraq.

2.3. Methods and processing procedure

In addition to the abovementioned challenges, one critical problem for salinity assessment by remote sensing is related to crop rotation/fallow practice which may lead to significant change in spectral reflectance and vegetation indices whereas salinity may not subsequently change. Therefore, a single date image cannot avoid such problem and is prone to giving false information on salinity. For this reason, we propose in this paper an innovative processing approach, that is, the multiyear maxima-based modeling approach for salinity mapping to minimize the aforementioned challenges or problematic issues based on the achievements of other authors (Hardisky et al., 1983; Zhang et al., 1997, 2011; Goossens and van Ranst, 1998; Eldeiry and Garcia, 2010; Garcia et al., 2005; Al-Khaier, 2003; Brunner et al., 2007; Iqbal, 2011). In this approach, only the maximal value of vegetation indices (VIs) or non-vegetation indices (NonVIs) of each pixel including both spring and summer in a period of four to five years was taken into consideration given that fallow lasts generally two to three years in Central Iraq. We assumed that salinity would not change significantly in such a short period if land use practice did not change. Then the maxima of vegetation indices were linked to the field-measured salinity (EM38 readings and laboratory EC) to derive remote sensing-based salinity models. The models were applied back to the maximal indices for salinity mapping in which vegetated and non-vegetated areas were separately treated. Such processing could also greatly resolve the gap problem in the recent Landsat ETM+ imagery (after 2003) left by the failure of the Scan-Line Corrector (SLC-Off) of the captor. The concrete procedures for image processing and modeling are unfurled in the following paragraphs.

2.3.1. Atmospheric correction and multispectral transformation

After conversion into at-satellite radiance, atmospheric correction of all Landsat, SPOT and RapidEye imagery was conducted using FLAASH (Fast Line-of-sight Atmospheric Analysis of Spectral Hypercubes) Model (Perkins et al., 2005) which can correct both additive and multiplicative atmospheric effects. FLAASH reflectance was rescaled to normal range of 0 to 1.

Multispectral transformation was undertaken on the atmospherically-corrected Landsat, SPOT and RapidEye images to derive a number of vegetation indices (VIs) that are considered useful for salinity assessment such as NDVI (Normalized Difference Vegetation Index: Rouse et al., 1973), SAVI (Soil Adjusted Vegetation Index: Huete, 1988), EVI (Enhanced Vegetation Index: Huete et al., 1997, 2002), ARVI (Atmospherically Resistant Vegetation Index) and SARVI (Soil-Adjusted and Atmospherically Resistant Vegetation Index: Kaufman and Tanré, 1992). We also used a new vegetation index, the Generalized Difference Vegetation Index (GDVI) developed by Wu (2014), for salinity analysis. The GDVI has the following form:

$$\mathrm{GDVI} = (SR^n - 1)/(SR^n + 1) = (\rho_{\mathrm{NIR}}^n - \rho_{\mathrm{R}}^n)/(\rho_{\mathrm{NIR}}^n + \rho_{\mathrm{R}}^n). \quad (1)$$

where SR is the simple ratio index; ρ_{NIR} and ρ_{R} are respectively the reflectance of the near infrared (NIR) and red (R) bands; and n is the power number, a non-zero integer from 1 to n. When $n = 1$, GDVI = NDVI. As Wu (2014) found, when $n = 2$, GDVI is better correlated with LAI (Leaf Area Index) in all biomes, and more sensitive to low vegetal biomes than all other vegetation indices. However, with the increase of n (e.g., $n = 3$ and 4), GDVI becomes saturated and insensitive to densely vegetated areas (e.g., wheat cropland, forest). High power GDVI is thence only relevant for land characterization in sparsely vegetated dryland biomes such as rangeland and woodland. Since there are different types of croplands in our study site, we applied GDVI, of which $n = 2$, as a test in this study to check its sensitivity to soil salinity together with other vegetation indices.

It is worthy of mention that SPOT and RapidEye images cannot provide VIs such as ARVI, EVI and SARVI as they do not contain the blue band.

The moisture/water content index, NDII (Hardisky et al., 1983), which is sensitive to not only canopy moisture but also salinity (negative relationship) due to the combination of TM band 5, was produced

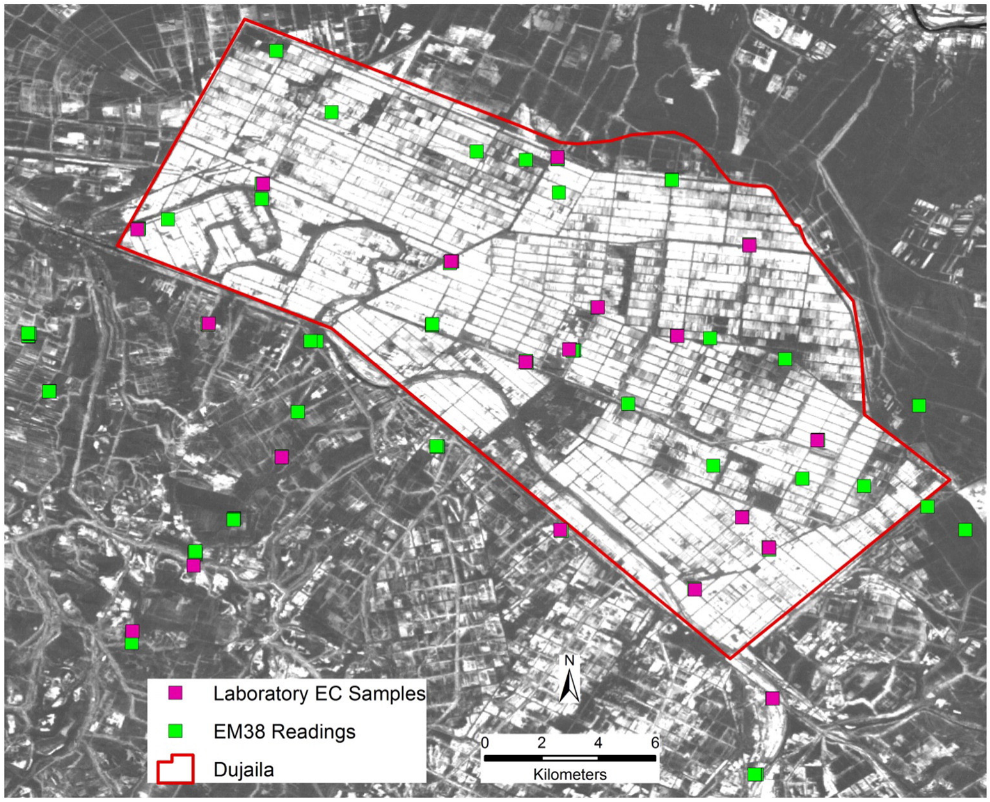

Fig. 2. Distribution of the field sampling plots. Note: The background is the multiyear maximal NDVI from Landsat ETM + images dated 2009–2012. (The SLC-Off gaps were filled. See Section 2.3 for procedure.)

from TM and SPOT 4 images, and other non-vegetation indices such as Tasseled Cap Brightness (TCB: Crist and Cicone, 1984; Huang et al., 2002; Ivits et al., 2008) and Principal Components (PCs, mainly the first and second Principal Components, denoted as PC1 and PC2) were also derived from Landsat TM and SPOT images (RapidEye can provide only PCs). These transformations convert land cover information from multispectral bands into several thematic indicators, e.g., vegetation greenness and soil moisture. Especially, TCB, an indicator of soil brightness, is regarded as an approximation of soil albedo or bulk reflectance.

LST, a useful salinity indicator as Metternicht and Zinck (1996, 2003), Goossens and van Ranst (1998) and Iqbal (2011) have revealed, was converted from the thermal band of Landsat TM and ETM + images during the crop growing period from February to the first half of April (because barley reaches its maturity in the middle of April and is harvested at the end of the month in Central and Southern Iraq). LST conversion was based on the following equations (Chander et al., 2009):

$$L_\lambda = G_{rescale} * Q_{cal} + B_{rescale} \tag{2}$$

$$T = K_2 / \ln\left((K_1/L_\lambda) + 1\right) \tag{3}$$

where L_λ is the spectral radiance at the sensor's aperture [W/(m^2 sr μm)]; Q_{cal} is the quantized calibrated pixel value in digital number [DN]; $G_{rescale}$ is the band-specific rescaling gain factor [(W/(m^2 sr μm))/DN]; $B_{rescale}$ is the band-specific rescaling bias factor [W/(m^2 sr μm)]; and K_1 and K_2 are calibration coefficients (see Chander et al., 2009 for detail).

2.3.2. Multiyear datasets and the maxima of VIs

A multiyear VI dataset including that from Landsat, SPOT and RapidEye images was constituted for each VI such as NDVI, SAVI, GDVI, EVI, and SARVI; the same was done for NDII and LST, and the NonVIs namely TCB and PCs (PC1 and PC2). Then the maximal value of each VI and NonVI in each pixel was extracted by an algorithm designed using IDL (Interactive Data Language).

To get a possibly better correlative function with salinity, the variants of the maximal indicators (VIs, NonVIs, NDII and LST) in the form of exponent (exp) and natural logarithm (ln) were derived in consideration of the fact that the dependent variable, in our case, the salinity, may have better response to the variant(s) of the independent variable(s).

Table 1
Landsat images in the frame with path-row number of 167-38 used in this study.

2010 (2009–2012) (Landsat 7 ETM+)		2000 (1998–2002) (Landsat 5 TM and 7 ETM+)		1990 (1988–1993) (Landsat 4 and 5 TM)	
Spring	Summer	Spring	Summer	Spring	Summer
2009-03-26	2009-09-02	1998-04-21 (L5)	1999-08-14 (L5)	1988-03-16 (L4)	1990-08-13 (L4)
2009-04-11	2010-08-20	2000-03-09 (L5)	2000-08-08 (L7)	1990-02-18 (L4)	1990-08-29 (L4)
2010-03-29	2011-08-23	2000-04-26 (L5)	2002-07-29 (L7)	1990-03-06 (L4)	1992-08-02 (L4)
2011-04-17	2012-08-25	2001-03-20 (L7)		1991-03-01 (L5)	1992-08-18 (L4)
2012-04-03		2001-04-21 (L7)		1993-02-26 (L4)	
2012-04-19		2002-04-24 (L7)		1993-03-30 (L4)	

2.3.3. Stratification of the vegetated and non-vegetated areas

To separate the vegetated and non-vegetated areas, we used the multiyear maximal NDVI image by thresholding technique, e.g., giving tentatively a threshold of 0.2 to examine whether it can divide largely the vegetated and non-vegetated areas while compared with the natural color composite of the original images. If the vegetated-area is overstated, the threshold should be tuned up (e.g., 0.21, 0.22), otherwise, it should be tuned down, e.g., 0.19, 0.18, till when the best threshold is reached. For the multiyear period 2009–2012, it is 0.23, and it is 0.21 for 1998–2002, and 0.22 for 1988–1993.

After this division, the sampled data located in different areas can be also divided into two groups: vegetated and non-vegetated area samples.

2.3.4. Multiple linear regression analysis

A Pearson correlation analysis was firstly applied to understand the correlation between the EC/EM38 and VIs/NonVIs or that among the VIs and NonVIs. Then the least-square multiple linear regression analysis was undertaken at the confidence level of 95% to couple the soil EC/EM38 measurements in 2011–2012 with the multiyear maximal VIs, NonVIs and their variants of the 2009–2012 period to obtain the specific salinity models in the vegetated area, and non-vegetated area, and the integrated salinity models in the whole study site including both vegetated and non-vegetated areas. We have to mention that the independent variables, which were strongly correlated with each other (e.g. $R^2 > 0.90$), were selectively input for modeling, i.e., we selected the ones of the best correlation with salinity among all the VIs, together with other non-correlated ones as inputs to avoid auto-correlation problem among VIs.

NDII and LST have both vegetation and non-vegetation characters, and were integrated in both vegetated and non-vegetated areas for salinity modeling.

2.3.5. Evaluation of the models' reliability

To understand whether all the models obtained in Section 2.3.4 are relevant, and reliable for predicting remote sensing-based salinity, it is essential to conduct an evaluation procedure to examine their predicted results against the field measured data. To achieve this purpose, the specific VI-based models were applied back to the maximal VIs in the vegetated area, and NonVI-based models to the maximal NonVIs in the non-vegetated area, and the integrated models to both VIs and NonVIs of the whole site of the period 2009–2012. The produced maps to be evaluated include (1) those from the integrated models EC-VIs and EM_V-VIs without distinction of vegetated and non-vegetated areas; (2) the mosaicked maps from the integrated models EC-VIs or EM_V-VIs for the vegetated area, and EM_V/EM_H-NonVIs for the non-vegetated area; and (3) the mosaicked ones from the specific models for vegetated and non-vegetated areas.

Theses maps were examined using laboratory measured salinity by linear regression analysis as was done by Wu et al. (2013) at the confidence level of 95%. If the agreement between the map and the ground truth data is >80% ($R^2 > 0.8$), the predicted salinity map is considered reliable and the models that we developed are operational.

2.3.6. Multitemporal mapping and salinity change trends

The most relevant salinity models that have been evaluated were applied to the historical multiyear maximal VIs and NonVIs dated 1990 (1988–1993) and 2000 (1998–2002) for multitemporal salinity mapping. As the processing of all historical images was the same as was done for the recent ones (the only difference is that there were no SPOT and RapidEye images in the historical datasets), the historical salinity maps were regarded reliable although we do not have much historical salinity measurement data to validate.

Based on this, the salinity dynamics, change trends in space and time in the recent decades, can be tracked by the differencing technique and the change in each salinity class was quantified.

2.3.7. Linking salinity change with land use practice and management

By linking the salinity maps and change trend with the field observation in land management and household socio-economic survey, a tentative analysis to understand the salinization process and causes was conducted.

3. Results and discussion

3.1. Salinity models

As shown in Table 2, all vegetation indices (including NDII and LST) and their exponential and logarithmic variants are strongly correlated with the salinity measured in laboratory (EC) and field EM38 readings if we take into account both vegetated and non-vegetated areas as a holistic site, and GDVI is the best salinity indicator. TCB and PCs, however, show lower correlations with EC and EM38 readings.

Table 3 shows that if we separate vegetated and non-vegetated areas, the correlation coefficients between EC/EM38 readings and VIs are generally low ($R^2 < 0.50$ for EC-VIs and <0.61 for EM_V/EM_H-VIs, respectively) in the vegetated area, and those in the non-vegetated area between EM_V/EM_H and NonVIs seem better, among which the best ones (e.g., EM_H-TCB/PC1) reach 0.74.

Multiple linear regression analysis allowed us to obtain a number of models as listed in Table 4: two integrated models (Model 1: EC-GDVI and Model 2: EM_V-GDVI) for the whole study site (without distinction of vegetated and non-vegetated areas), two integrated models (Model 3: EM_V-LST/NDII and Model 4: EM_H-LST/NDII) for the non-vegetated area in which all samples were calibrated with the NonVIs, one specific model for the vegetated area (Model 5: EM_V-GDVI) based on 43 samples located in the vegetated area, and two specific models (Model 6: EM_V-PC1 and Model 7: EM_H-TCB) for non-vegetated areas which were derived from 16 samples in the non-vegetated area.

The predicted salinity of the whole study area by Models 1 and 2 was evaluated with the ground measured data (laboratory EC), and the results are shown in Fig. 3a and b. Clearly, both models allow predictions with high accuracy ($R^2 = 0.864$ from Model 1 and $R^2 = 0.869$ from Model 2). However, the salinity predicted from Model 2 (EM_V-GDVI) has a clear shift from the ground measured salinity by 8.99 — the intercept in Fig. 3b, which means that the modeled ECs from Model 2 (EM_V-GDVI) are higher than the ground measured ones as a consequence of multiplicative error from EM_V-GDVI to EC-EM_V. To match the salinity map derived from the EM_V-VIs model (Model 2) to the real salinity, there is a need to adjust this shift by reducing $8.99 - 0.59 = 8.4$ to keep it at the same level as that from Model 1 (EC-GDVI), of which the intercept is 0.59. The advantage of these two models lies in the reasonable prediction in the vegetated area but the disadvantage is the underestimation of Model 1 and overestimation of Model 2 in the non-vegetated area, e.g., about 15–40 dS/m lower in the strongly salinized area for Model 1 and 10–35 dS/m higher in the known sampling sites in the non-vegetated area for Model 2 despite their globally high multiple R^2 values.

For this reason, other two salinity maps from Models 3 and 4 were produced for the non-vegetated area. After the shift adjustment, 1500 random points were generated in the non-vegetated area to check the agreement between the two maps. By removing those falling in the SLC-Off gaps (although we have applied the multiyear maximal algorithm, gaps cannot be perfectly filled in the LST and NDII images), 1186 points remained. The predicted EC values of both salinity maps at these points were extracted for the non-vegetated area. The agreement between two maps was found to be very high (Fig. 3c, $R^2 = 0.944$), whereas, Model 4 seems slightly overestimated with respect to the known salinity. So, the map from Model 3 appears more relevant for the non-vegetated area.

As for the specific Model 5 (EM_V-GDVI, where the multiple R^2 value is low, 0.372), the salinity map was produced for the vegetated area, and its agreement with or its reliability against the ground data is about

Table 2
Integrated Pearson correlation coefficients between salinity and VIs/NonVIs in both vegetated and non-vegetated areas in the whole Dujaila site.

Cases (N)	Salinity	SAVI	SARVI	NDVI	GDVI	EVI	NDII	ln(SAVI)	ln(SARVI)	ln(NDVI)	ln(GDVI)	ln(EVI)	ln(NDII)
20	EC	−0.799	−0.811	−0.829	−0.867	−0.761	−0.807	−0.869	−0.881	−0.891	−0.899	−0.869	−0.891
59	EM_V	−0.824	−0.820	−0.837	−0.858	−0.798	−0.779	−0.836	−0.786	−0.847	−0.837	−0.825	−0.783
59	EM_H	−0.791	−0.781	−0.806	−0.838	−0.759	−0.740	−0.820	−0.757	−0.831	−0.829	−0.798	−0.743

Cases (N)	Salinity	exp(GDVI)	exp(NDVI)	exp(EVI)	exp(SAVI)	LST	ln(LST)	PC1	PC2	TCB
20	EC	−0.840	−0.802	−0.678	−0.777	0.711	0.712	0.495	0.403	0.470
59	EM_V	−0.854	−0.818	−0.733	−0.809	0.633	0.633	0.638	0.565	0.594
59	EM_H	−0.828	−0.783	−0.689	−0.773	0.651	0.650	0.591	0.556	0.592

37.7%. Thus, Model 5 is not recommended to derive salinity map for vegetated area.

Regarding the specific models for non-vegetated areas, Model 6 (EM_V-PC1) has the same problem as Model 5, i.e., low multiple R^2. This constitutes the limitation of the model to be applied in the non-vegetated area. Model 7 (EM_H-TCB) seems to be in a better situation and reveals well the relationship between salinity and TCB, a representative of the holistic reflectance or albedo of the non-vegetated area. However, the derived salinity map shows some unrealistic salinity in saline bareland. For example, the predicted salinity by this model is relatively low in the salt accumulated area (seen white in the color composites) where the salinity should be theoretically high. Probably, this problem is due to the low representativeness of samples in the non-vegetated area. This model is hence not recommended for the derivation of salinity map in the non-vegetated area.

Based on the foregoing evaluation, we understand that the integrated Models 1 and 2 are reasonable for the vegetated area, Model 1 does not need the shift correction and is the preferred one, and Model 3 is pertinent for non-vegetated area. We selected Models 1 and 3 to produce a mosaicked salinity map of the Dujaila area. The accuracy of this map against the ground measured salinity is 82.57% (Fig. 3d), a bit lower than those directly from Models 1 and 2 (Fig. 3a and b), and the salinity in the non-vegetated area of this map seems more appropriate according to our knowledge. The combination of Models 1 and 3 is thus considered operational for Central Iraq.

3.2. Salinity maps and change trend analysis

As a result of the application of Models 1 and 3 to the historical multiyear maximal GDVI, LST and NDII dated 1990 and 2000, we obtained the mosaicked salinity maps of 1990 and 2000. These maps together with that of 2010 are presented in Fig. 4. The salinity change trend was highlighted by using the differencing technique (Fig. 5), and salinization at different levels is quantified and shown in Table 5.

As shown in Fig. 5 and Table 5, the salinity of different levels has experienced a strong dynamic change. From 1990 to 2000, both slightly and moderately salinized land increased respectively by 188% and 150% at the cost of non-saline land (which was reduced by about 29%). Such intensification of salinity is a consequence of land use and management of local farmers related to the macroscopic environment in Iraq. After the Gulf War during 1990–1991, Iraq was under economic sanction by the United Nations (UNSC Resolution 660: http://www.un.org/en/sc/documents/resolutions/1990.shtml). This forced local farmers to increase land area to produce sufficient amount of food to meet the needs of the country, and different land management practices were carried out. However, the maintenance of the existing irrigation–drainage system, which is the guaranty of the crop production in a dry environment and removes salt from soils, and the reparation of the system damaged by the war, could not be supported due to the constraint of economic conditions, not to mention to develop new irrigation–drainage systems. That is why slight and moderate salinization had extended in Dujaila.

Post 2000, a part of the irrigation–drainage system and other infrastructures were further devastated, and agricultural activities became impossible for most of the farmers in Central and Southern Iraq. In the post-war time (after 2003), international communities and stakeholders including a number of UN agencies started to intervene in the form of humanitarian aid and investment for reconstruction of the country (http://fpc.state.gov/documents/organization/50252.pdf). This has led to a certain improvement of the harsh condition, e.g., restoration of parts of damaged canals, and possibility to import food from outside. A part of slightly and moderately salinized croplands were turned into non-saline land again thanks to the recovery of the irrigation–drainage system. Nonetheless, other farmers, who could not benefit from this limited improvement, left their land uncultivated due to the poor socio-economic conditions and the necessity for huge investment to control the salinity and at the same time to recover the irrigation–drainage systems. The non-availability of the necessary agricultural system and land abandonment has led to elevation of the groundwater table near to the surface exacerbating salt accumulation and salinization in the soils. That is why the strongly and extremely salinized classes have increased in the Dujaila site from 2000 to 2010 (Table 5).

Apart from the regional socio-economic conditions related to salinization in the region, our field survey in this site revealed some microscopic phenomena related to salinization. For example, salts are easily gathered in certain drainage ditches, non-reclaimed areas and abandoned river course transported by the drainage systems. When the drainage system gets damaged, and land abandoned, salts are accumulated directly in

Table 3
Pearson correlation coefficients between EC/EM38 readings and VIs in vegetated areas and between EC/EM38 and NonVIs in non-vegetated areas.

	Cases (N)	Salinity	SAVI	ln(SAVI)	EVI	ln(EVI)	NDVI	ln(NDVI)	GDVI	ln(GDVI)	NDII	ln(NDII)	SARVI	ln(SARVI)
Vegetated area	14[a]	EC	−0.314	−0.288	−0.372	−0.36	−0.387	−0.375	−0.379	−0.364	−0.464	−0.42	−0.447	−0.454
	43[b]	EM_V	−0.556	−0.564	−0.540	−0.535	−0.588	−0.602	−0.607	−0.61	−0.478	−0.478	−0.555	−0.555
	43[b]	EM_H	−0.462	−0.468	−0.457	−0.453	−0.508	−0.524	−0.532	−0.537	−0.389	−0.389	−0.471	−0.473

	Cases (N)	Salinity	PC1	PC2	TCB	LST	ln(TCB)	exp(TCB)	exp(PC1)	exp(PC2)
Non-vegetated area	16[c]	EM_V	−0.666	−0.263	−0.645	−0.048	−0.643	−0.646	−0.667	−0.263
	16[c]	EM_H	−0.737	−0.127	−0.742	−0.030	−0.746	−0.739	−0.734	−0.128

[a] 14 of 20 laboratory measured soil salinity samples are situated in the vegetated area.
[b] 44 pairs of EM38 readings in total fall in the vegetated area but one is an outlier.
[c] 18 pairs of field EM38 readings (EM_V and EM_H) are located in the non-vegetated area but 2 cases are not usable because of the difficulty of zeroing (to adjust the background signal of the EM38 instrument to zero).

Table 4
Remote sensing-based salinity models.

Type	Model no.	Models	Equations	Error scope	Multiple R^2	F-ratio	p-Value	Cases (N)
Integrated models for both vegetated area	1	EC-GDVI	$EC = -2.87 - 23.27\ \ln(GDVI)$ (dS/m)	±5.240	0.874	111.137	1.31E−08	19[a]
and non-vegetated areas	2	EM_V-GDVI	$EM_V = 535.403 - 487.905GDVI$ (mS/m)	±64.168	0.729	142.839	9.99E−16	58[b]
Integrated models for non-vegetated area	3	EM_V-LST/NDII	$EM_V = -2725.05 + 10.018LST - 509.494NDII$ (mS/m)	±73.230	0.650	47.360	2.36E−12	58[b]
	4	EM_H-LST/NDII	$EM_H = 1,627,956.14 + 1148.84LST - 345,815.62\ \ln(LST) - 245.198NDII$ (mS/m)	±58.240	0.649	30.869	1.95E−11	58[b]
Vegetated area specific model	5	EM_V-GDVI	$EM_V = 64.359 - 319.306\ \ln(GDVI)$ (mS/m)	±54.680	0.372	24.331	1.39E−05	43
Non-vegetated area specific models	6	EM_V-PC1	$EM_V = 1502.43 - 1166.35\ \exp(PC1)$ (mS/m)	±90.811	0.444	11.200	0.005	16
	7	EM_H-TCB	$EM_H = -223.22 - 1043.11\ \ln(TCB)$ (mS/m)	±74.549	0.557	17.585	0.001	16

EM_V/EM_H (mS/m) can be converted into soil electrical conductivity (EC in dS/m) by the following relationships obtained from the regional transect sampling and measurement in Mesopotamia: $EC = 0.0005EM_V^2 - 0.0779EM_V + 12.655$ ($R^2 = 0.850$) and $EC = 0.0002EM_H^2 + 0.0956EM_H + 0.0688$ ($R^2 = 0.791$).
[a] Model was obtained with 19 samples after removing one outlier.
[b] Three non-zeroing cases and one outlier were removed.

the fields as a consequence of groundwater table rise or drying-up of the logged saline waters. In fact, the concentration of salt(s) in groundwater in most areas in Central Iraq reaches about 10,000 to 100,000 ppm, and locally, up to 120,000 ppm. Without an efficient irrigation–drainage system, salts are released and accumulated in the soils after evaporation. This may be the reason explaining the increase in salinity in the north (abandoned and uncultivated areas in the recent years) and the central south (non-reclaimed area) part of the study site. Our socio-economic investigation based on 150 household questionnaires reveals that the dominant driver of salinization and the most difficult factor to control salinity are the absence of efficient and modern irrigation–drainage systems (97.5%) and the present irrigation manner such as flooding irrigation is harmful. Therefore, the restoration or improvement of the available systems or development of the new systems is the pressing issue for the local governments and farmers, which needs investment from the central government or international consortiums.

3.3. Relevance of the mapping methodology and its advantages

As demonstrated in Section 2, the proposed methodology including derivation of the multiyear maximal remote sensing indicators and multivariate regression modeling allows us to achieve the development of salinity models, multitemporal mapping and quantification with rather considerable reliability and accuracy. However, the following points are worthy of attention.

After application of the multiyear maxima-based modeling approach, influence of crop rotation and fallow – false alarm on salinity which is inevitable when using single image – is excluded as the maximal VI can be considered as an integrated proxy of the best crop performance. Actually, the greenness of a given crop in the single image is easily subject to the impacts from the biotic and abiotic stresses such as outbreaks of disease or rust, moisture, soil fertility as well as soil salinity. With this new processing algorithm, the moisture-, fertility- and disease-related stresses,

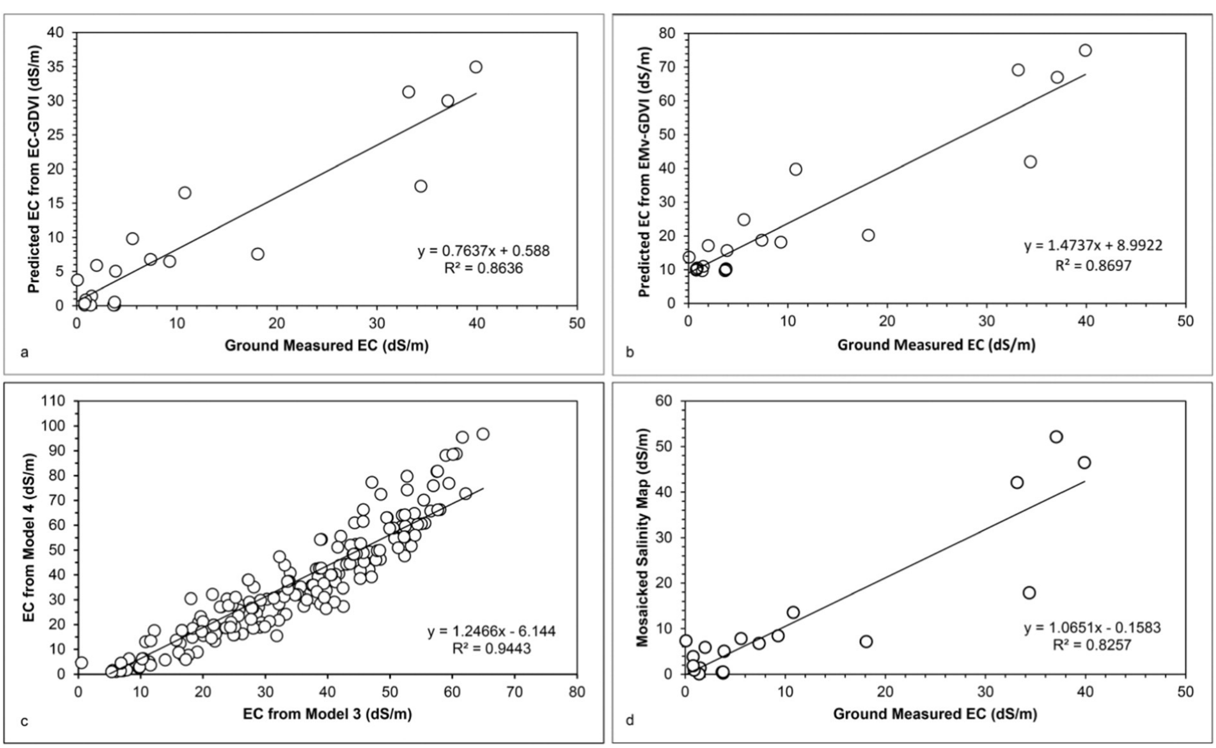

Fig. 3. Reliability of the predicted salinity. Note: (a) and (b) show respectively the agreement of the predicted salinity from Model 1 (EC-GDVI) and Model 2 (EM_V-GDVI) with the ground measured salinity in the whole study area; (c) reveals the similarity and difference between the predicted EC from Models 3 and 4 in the non-vegetated area; and (d) shows the reliability of the mosaicked salinity map of 2010 against the ground measured data.

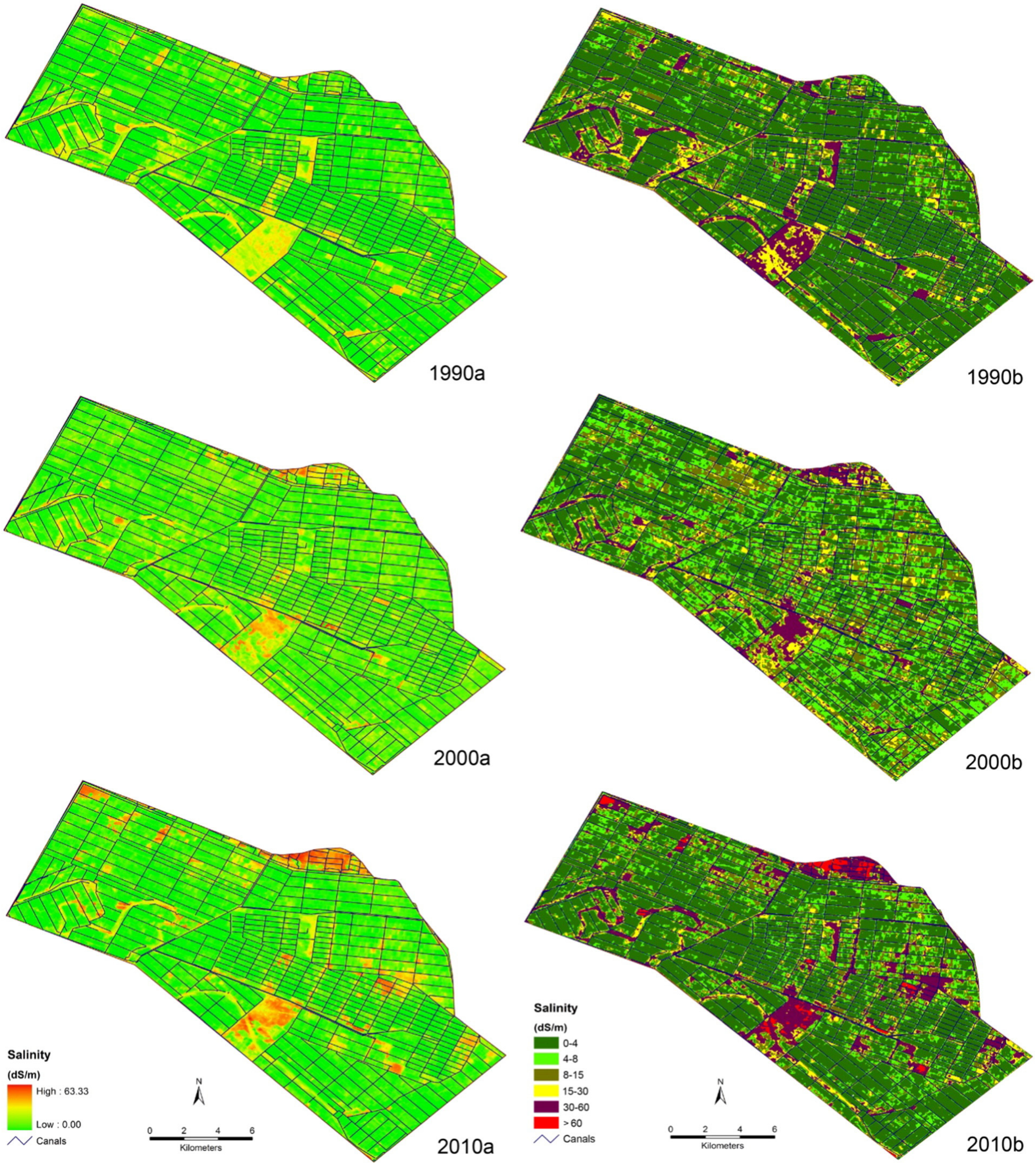

Fig. 4. Multitemporal salinity maps of the Dujaila pilot site. Left: (a) maps are expressed in hue-saturation, and right: (b) maps are shown in salinity level as required by land users and managers.

which may cause confusion as salinity, can be minimized because during the 4-year period, there would be at least one crop (either in spring or summer) that could have normally grown without water, fertility and disease stresses if soil condition did not change and there was no sudden change in land use and management in the given patch of land.

For the non-vegetated area, the moisture problem has been also minimized or avoided and reflectance maximized as we took the maximal NonVIs (e.g., TCB, LST and NDII). It is known that the higher temperature corresponds to lower moisture in soils (Qiu, 2006), and the higher soil brightness (TCB) to higher soil albedo or bulk reflectance. The problematic issues mentioned in Section 1 were thus resolved.

The shortcoming that still remains is that related to the salt-tolerant crops such as barley, alfalfa and cotton. Halophytes can be easily recognized as they are mostly distributed along the banks of the drainage channels or near or in the swamps, but barley and cotton are cultivated in croplands. As was revealed by the experiments conducted by Dieleman (1963), barley has a rather strong resistance to salinity, and can still grow well with good production (1.68–1.84 tons/ha) in the fields where soil salinity reaches 8–16 dS/m if fertilizer (e.g., nitrogen) is available. So visually, barley appears as strong greenness in satellite imagery and this tends to give us a false appearance of very low salinity in images (e.g., <4 dS/m). Despite the application of the multiyear

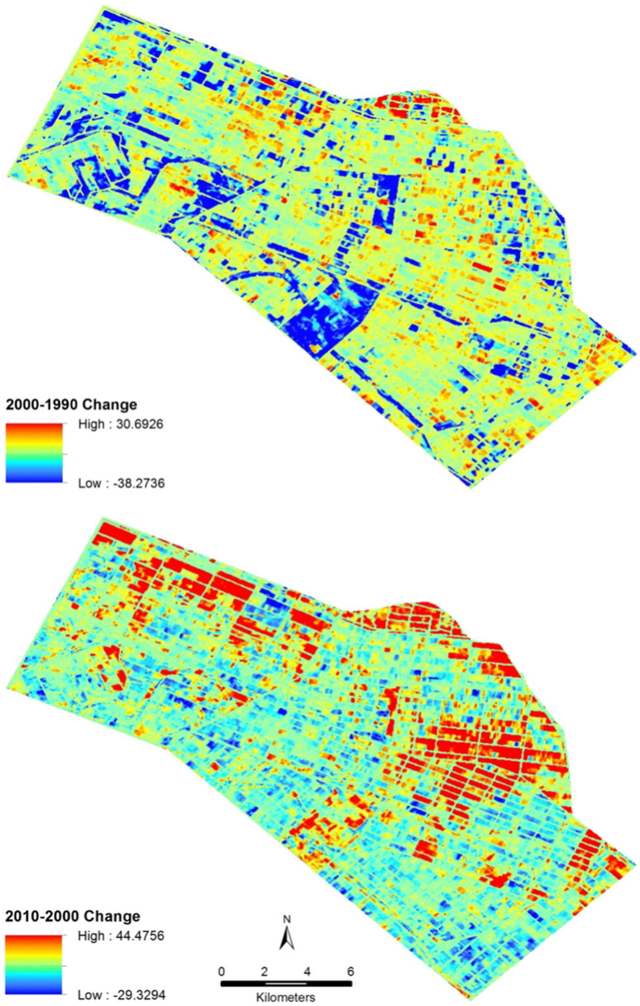

Fig. 5. Salinity change trends in Dujaila. Red (positive change) indicates an increase in salinity, and blue (negative change), a decrease in salinity in the observation periods from 1990 to 2000 and from 2000 to 2010.

maxima-based algorithm, such "false salinity" may not be completely removed.

One may understand the relevance of VIs and other NonVIs such as TCB for salinity assessment but have concern about the reasonability to use LST as one of the salinity indicators in bareland. In fact, it is a common knowledge that thermal conductivity of materials is temperature (T) dependent, and the former is associated with electrical conductivity (EC). This provides a possibility to quantify the salinity by using soil T, in this case, LST. However, the interrelationship between the thermal and electrical conductivities is complex and may change significantly depending on materials, e.g., soil types. Mougenot et al. (1993), Metternicht and Zinck (1996), Goossens and van Ranst (1998), and Iqbal (2011) have explored the possibility to use the thermal band to identify the salt-affected soils or to differentiate saline soil from gypsiferous soils, but they have not discussed the mechanism behind. Abu-Hamdeh and Reeder (2000) ascertained the relationship between thermal conductivity and salinity, and found that thermal conductivity decreases with the increase in the amount of added salts at given moisture content. Sepaskhah and Boersma (1979) found that the apparent thermal conductivity is independent of water content at very low water contents. Consequently, in the driest condition (lowest moisture), thermal conductivity is associated with the salt amount — salinity. We believe, therefore, that LST-based models are relevant.

Concern on the applicability of the models may also be addressed. Since the models were obtained from a pilot site study, direct extension without necessary adjustment or adaptation to other dry areas is not recommended. However, we consider it reasonable to extend our salinity mapping methodology as the challenges and problematic issues that are commonly faced in salinity mapping by remote sensing are minimized. In fact, Douaoui et al. (2006), Fernández-Buces et al. (2006), Brunner et al. (2007) and Eldeiry and Garcia (2010) have conducted different modeling and best band combinations for salinity mapping studies, but they used single or multiple single images and did not treat differently the vegetated and non-vegetated areas. Especially, Eldeiry and Garcia (2010) did not take into account the non-vegetated area. Their approaches cannot avoid the influences from crop rotation/fallow, and moisture.

To test the applicability of the methodology, we applied the same approach and procedure to another pilot site, Musaib, in Mesopotamia for multitemporal salinity mapping, and the assessment work was successfully achieved (Mhaimeed et al., 2013). Therefore, we believe that the approaches that we proposed in this paper are extendable to other similar environments for salinity mapping and assessment.

4. Conclusions

This paper demonstrates salinity mapping and change trend analysis in Dujaila in Central Iraq based on the development of relevant salinity models and mapping approaches despite the challenges and difficulty. Although more field data and good quality satellite imagery containing both middle infrared and thermal bands are needed for wider validation and improvement of the maps and models, the map of the present state is in good agreement with the field measurements. This implies that the models developed are operational in Dujaila and our methodology, of evident advantages and its uniqueness from others, is extendable to other similar dryland environments for salinity assessment.

It is seen that the salinity has experienced significant changes in Dujaila in the past decades which are closely related to land use and management (e.g., land abandonment) by farmers that are associated with both macro- and micro-socioeconomic environments in Iraq apart from the natural factors such as high salt concentration of groundwater, and dry climate. For better understanding of the causes of salinization, a spatially explicit modeling incorporating natural, socioeconomic, and climate data to reveal both the spatial and human determinants and the impacts of climate change on salinization is required in the future.

The real difficulty that we faced was the field sampling and the lack of good quality satellite images for the recent years. Due to security

Table 5
Salinity change trends in the Dujaila site.

Salinity level (dS/m)	Area (ha)			Change trend			
	1990	2000	2010	Change from 1990 to 2000 (ha)	% of change vs. 1990	Change from 2000 to 2010 (ha)	% of change vs. 2000
0.0–4.0 (non-saline)	19,394	13,787	17,707	−5607	−28.9	3921	28.4
4.0–8.0 (slightly)	2018	5818	2924	3800	188.4	−2894	−49.7
8.0–15.0 (moderately)	1600	4012	2021	2412	150.8	−1991	−49.6
15.0–30.0 (strongly)	2084	1568	1303	−516	−24.8	−265	−16.9
30.0–60.0 (very strongly)	718	630	1854	−88	−12.3	1225	194.6
>60.0 (extremely)	0	0	3	0	0	3	0

reasons, a number of designed sampling plots were not accessible, especially in barelands. Instead of random sampling, a stratified sampling is envisaged when the security situation improves. Additionally, Landsat ETM+ images were the main source that we could utilize for the recent period. Due to the SLC-Off problem, these images, especially, the shortwave infrared and thermal bands were not ideal though we had applied the maxima-based algorithm. In future work, we should use Landsat 8 data as they have become available since April 2013.

Acknowledgments

The study was funded by the Australian Centre for International Agricultural Research (ACIAR) [Project No: LWR/2009/034]. All Landsat images were freely obtained from the USGS data server (http://glovis.usgs.gov). The RapidEye image was provided by Mr Clemens Stromeyer (RapidEye AG). A sincere thank is due to Dr Ayad A. Hameed, Dr Hassan H. Al-Musawi (Ministry of Water Resources of Iraq), and Ms Binan Dardar (ICARDA) for their assistance in field sampling and partially image processing. Gratitude will also go to Dr Kasim A. Saliem (Ministry of Agriculture of Iraq), Mr Alexander Platonov (IWMI-Tashkent), Dr Evan Christen (CSIRO), Dr Manzoor Qadir (UNU-INWEH), and Dr Theib Oweis (ICARDA) for their cooperation in the early stage of the work.

Appendix A. Supplementary data

Supplementary data associated with this article can be found in the online version, at http://dx.doi.org/10.1016/j.geodrs.2014.09.002. These data include Google maps of the most important areas described in this article.

References

Abood, S., Maclean, A., Falkowski, M., 2011. Soil salinity detection in the Mesopotamian agricultural plain utilizing WorldView-2 imageryAvailable at: http://dgl.us.neolane.net/res/img/16bb89b080930a8ad1fdfc17665883e9.pdf.

Abu-Hamdeh, N.H., Reeder, R.C., 2000. Soil thermal conductivity effects of density, moisture, salt concentration, and organic matter. Soil Sci. Soc. Am. J. 64, 1285–1290. http://dx.doi.org/10.2136/sssaj2000.6441285x.

Al-Khaier, F., 2003. Soil Salinity Detection Using Satellite Remote Sensing(MS Thesis) ITC (International Institute for Geo-information Science and Earth Observation), The Netherlands.

Al-Layla, M.A., 1978. Effect of salinity on agriculture in Iraq. J. Irrig. Drain. Div. 104 (2), 195–207.

Al-Mahawili, S.M.H., 1983. Satellite Image Interpretation and Laboratory Spectral Reflectance Measurement of Saline and Gypsiferous Soils of West Baghdad(M.Sc Thesis) Purdue University, Iraq.

Brunner, P., Li, H.T., Kinzelbach, W., Li, W.P., 2007. Generating soil electrical conductivity maps at regional level by integrating measurements on the ground and remote sensing data. Int. J. Remote Sens. 28, 3341–3361.

Buringh, P., 1960. Soils and Soil Conditions in Iraq. Ministry of Agriculture of Iraq, (337 pp.).

Chander, G., Markham, B.L., Helder, D.L., 2009. Summary of current radiometric calibration coefficients for Landsat MSS, TM, ETM+, and EO-1 ALI sensors. Remote Sens. Environ. 113, 893–903.

Crist, E.P., Cicone, R.C., 1984. Application of the tasseled cap concept to simulated thematic mapper data. Photogramm. Eng. Remote. Sens. 50, 343–352.

Dieleman, P.J. (Ed.), 1963. Reclamation of Salt Affected Soils in Iraq. International Institute for Land Reclamation and Improvement, Wageningen Publication (175 pp.).

Douaoui, A.E.K., Nicolas, H., Walter, C., 2006. Detecting salinity hazards within a semiarid context by means of combining soil and remote-sensing data. Geoderma 134, 217–230.

Driessen, P.M., Schoorl, R., 1973. Mineralogy and morphology of salt efflorescences on saline soils in the Great Konya Basin, Turkey. J. Soil Sci. 24, 436–442.

Eldeiry, A.A., Garcia, L.A., 2010. Comparison of ordinary kriging, regression kriging, and cokriging techniques to estimate soil salinity using Landsat images. J. Irrig. Drain. Eng. 136, 355–364.

Epema, G.F., 1990. Effect of moisture content on spectral reflectance in a playa area in southern Tunisia. Proc. International Symposium on Remote Sensing and Water Resources, Enschede. International Institute for Aerospace Survey and Earth Sciences, The Netherlands, pp. 301–308.

FAO, 2008. Irrigation in the Middle East Region in figures. FAO Water Reports 34. AQUASTAT Survey, p. 423.

FAO, 2011. Country Pasture/Forage Resource Profiles: Iraq. FAO, Rome, Italy, p. 34.

Farifteh, J., Farshad, A., George, R.J., 2006. Assessing salt-affected soils using remote sensing, solute modelling, and geophysics. Geoderma 130 (3–4), 191–206.

Farifteh, J., van der Meer, F., Atzberger, C., Carranza, E., 2007. Quantitative analysis of salt-affected soil reflectance spectra: a comparison of two adaptive methods (PLSR and ANN). Remote Sens. Environ. 110, 59–78.

Fernández-Buces, N., Siebe, C., Cram, S., Palacio, J.L., 2006. Mapping soil salinity using a combined spectral response index for bare soil and vegetation: a case study in the former lake Texcoco, Mexico. J. Arid Environ. 65, 644–667.

Furby, S., Caccetta, P., Wallace, J., 2010. Salinity monitoring in Western Australia using remotely sensed and other spatial data. J. Environ. Qual. 39, 16–25.

Garcia, L., Eldeiry, A., Elhaddad, A., 2005. Estimating soil salinity using remote sensing data. Proceedings of the 2005 Central Plains Irrigation Conference, pp. 1–10 (available at: http://www.ksre.ksu.edu/irrigate/OOW/P05/Garcia.pdf; accessed on Jan 2013).

Ghabour, T.K., Daels, L., 1993. Mapping and monitoring of soil salinity of ISSN. Egypt. J. Soil Sci. 33 (4), 355–370.

Golovina, N.N., Minskiy, D., Pankova, Y., Solovyev, D.A., 1992. Automated air photo interpretation in the mapping of soil salinization in cotton-growing zones. Mapp. Sci. Remote. Sens. 29, 262–268.

Goossens, R., van Ranst, E., 1998. The use of remote sensing to map gypsiferous soils in the Ismailia Province (Egypt). Geoderma 87, 47–56.

Hardisky, M.A., Klemas, V., Smart, R.M., 1983. The influences of soil salinity, growth form, and leaf moisture on the spectral reflectance of Spartina alterniflora canopies. Photogramm. Eng. Remote Sens. 49, 77–83.

Hu, W., Shao, M.A., Wan, L., Si, B.C., 2014. Spatial variability of soil electrical conductivity in a small watershed on the Loess Plateau of China. Geoderma 230–231, 212–220.

Huang, C., Wylie, B., Yang, L., Homer, C., Zylstra, G., 2002. Derivation of a tasseled cap transformation based on Landsat 7 at-satellite reflectance. Int. J. Remote Sens. 23, 1741–1748.

Huete, A.R., 1988. A soil adjusted vegetation index (SAVI). Remote Sens. Environ. 25, 295–309.

Huete, A.R., Liu, H.Q., Batchily, K., van Leeuwen, W., 1997. A comparison of vegetation indices global set of TM images for EOS-MODIS. Remote Sens. Environ. 59, 440–451.

Huete, A.R., Didan, K., Miura, T., Rodriguez, E.P., Gao, X., Ferreira, L.G., 2002. Overview of the radiometric and biophysical performance of the MODIS vegetation indices. Remote Sens. Environ. 83, 195–213.

Hunt, G., Salisbury, J., Lenhoff, C., 1972. Visible and near infrared spectra of minerals and rocks: V. Halides, phosphates, arsenates, venadates and borates. Mod. Geol. 3, 121–132.

Iqbal, F., 2011. Detection of salt affected soil in rice–wheat area using satellite image. Afr. J. Agric. Res. 6, 4973–4982.

Ivits, E., Lamb, A., Langar, F., Hemphill, S., Koch, B., 2008. Orthogonal transformation of segmented SPOT5 images: seasonal and geographical dependence of the tasselled cap parameters. Photogramm. Eng. Remote Sens. 74 (11), 1351–1364.

Jacobsen, T., Adams, R.M., 1958. Salt and silt in ancient Mesopotamian agriculture. Science 128, 1251–1258.

Kaufman, Y.J., Tanré, D., 1992. Atmospherically resistant vegetation index (ARVI) for EOS-MODIS. IEEE Trans. Geosci. Remote Sens. 30, 261–270.

Lobell, D.B., Lesch, S.M., Corwin, D.L., Ulmer, M.G., Anderson, K.A., Potts, D.J., Doolittle, J.A., Matos, M.R., Baltes, M.J., 2010. Regional-scale assessment of soil salinity in the red river valley using multi-year MODIS EVI and NDVI. J. Environ. Qual. 39, 35–41.

Metternicht, G., 1998. Analysing the relationship between ground based reflectance and environmental indicators of salinity processes in the Cochabamba Valleys (Bolivia). Int. J. Ecol. Environ. Sci. 24, 359–370.

Metternicht, G.I., Zinck, J.A., 1996. Modelling salinity–alkalinity classes for mapping salt-affected topsoils in the semi-arid valleys of Cochabamba (Bolivia). ITC J. 1996 (2), 125–135.

Metternicht, G.I., Zinck, J.A., 2003. Remote sensing of soil salinity: potentials and constraints. Remote Sens. Environ. 85, 1–20.

Mhaimeed, A., Wu, W., AL-Shafie, W., Ziadat, F., Al-Musawi, H., Kasim, A.S., 2013. Use remote sensing to map soil salinity in the Musaib Area in Central Iraq. Int. J. Geosci. Geomatics 1 (2), 34–41 (ISSN 2052-5591).

Mougenot, B., Pouget, M., Epema, G., 1993. Remote sensing of salt-affected soils. Remote Sens. Rev. 7, 241–259.

Perkins, T., Adler-Golden, S., Matthew, M., Berk, A., Anderson, G., Gardner, J., Felde, G., 2005. Retrieval of atmospheric properties from hyper and multispectral imagery with the FLAASH atmospheric correction algorithm. In: Schäfer, K., Comerón, A.T., Slusser, J.R., Picard, R.H., Carleer, M.R., Sifakis, N. (Eds.), Remote Sensing of Clouds and the Atmosphere X. Proceedings of SPIE vol. 5979.

Qiu, H., 2006. Thermal remote sensing of soil moisture: validation of presumed linear relation between surface temperature gradient and soil moisture contentAvailable at: http://people.eng.unimelb.edu.au/jwalker/theses/HuangQui.pdf.

Rao, B., Sankar, T., Dwivedi, R., Thammappa, S., Venkataratnam, L., Sharma, R., Das, S., 1995. Spectral behaviour of salt-affected soils. Int. J. Remote Sens. 16, 2125–2136.

Rodríguez, P.G., González, M.E.P., Zaballos, A.G., 2007. Mapping of salt-affected soils using TM images. Int. J. Remote Sens. 28, 2713–2722.

Rouse, J.W., Haas, R.H., Schell, J.A., Deering, D.W., 1973. Monitoring vegetation systems in the Great Plains with ERTS. Proceedings of the Third ERTS-1 Symposium. NASA SP-351 1, pp. 309–317.

Schnepf, R., 2004. Iraq agriculture and food supply: background and issues, Congressional Research Service. The Library of Congress (62 pp.).

Sepaskhah, A.R., Boersma, L., 1979. Thermal conductivity of soils as a function of temperature and water content. Soil Sci. Soc. Am. J. 43 (3), 439–444. http://dx.doi.org/10.2136/sssaj1979.03615995004300030003x.

Shao, Y., Hu, Q., Guo, H., Lu, Y., Dong, Q., Han, C., 2003. Effect of dielectric properties of moist salinized soils on backscattering coefficients extracted from RADARSAT image. IEEE Trans. Geosci. Remote Sens. 41, 1879–1888.

Singh, R.P., Srivastav, S.K., 1990. Mapping of waterlogged and salt affected soils using microwave radiometers. Int. J. Remote Sens. 11, 1879–1887.

Singh, R., Kumar, V., Srivastav, S., 1990. Use of microwave remote sensing in salinity estimation. Int. J. Remote Sens. 11, 321–330.

Steven, M.D., Malthus, T.J., Jaggard, F.M., Andrieu, B., 1992. Monitoring responses of vegetation to stress. In: Cracknell, A.P., Vaughan, R.A. (Eds.), Remote Sensing from Research to Operation: Proceedings of the 18th Annual Conference of the Remote Sensing Society. United Kingdom.

Taylor, G.R., Mah, A.H., Kruse, F.A., Kierein-Young, K.S., Hewson, R.D., Bennett, B.A., 1996. Characterization of saline soils using airborne radar imagery. Remote Sens. Environ. 57, 127–142.

Wu, W., 2014. The generalized difference vegetation index (GDVI) for dryland characterization. Remote Sens. 6, 1211–1233.

Wu, W., De Pauw, E., Hellden, U., 2013. Assessing woody biomass in African tropical savannahs by multiscale remote sensing. Int. J. Remote Sens. 34, 4525–4529.

Zhang, M., Ustin, S., Rejmankova, E., Sanderson, E., 1997. Monitoring Pacific coast salt marshes using remote sensing. Ecol. Appl. 7, 1039–1053.

Zhang, T., Zeng, S., Gao, Y., Ouyang, Z., Li, B., Fang, C., Zhao, B., 2011. Using hyperspectral vegetation indices as a proxy to monitor soil salinity. Ecol. Indic. 11, 1552–1562.